Soft Robotic Fingers with Embedded Ionogel Sensors and Discrete Actuation Modes for Somatosensitive Manipulation

Ryan L. Truby[1,2,*], Robert K. Katzschmann[2], Jennifer A. Lewis[3,*], and Daniela Rus[2,*]

Abstract—Soft robotic grippers enable gentle, adaptive, and bioinspired manipulation that is simply not possible using traditional rigid robots. However, it has remained challenging to create multi-degree-of-freedom soft actuators with appropriate sensory capabilities for soft manipulators requiring greater dexterity and closed-loop control. In this work, we use embedded 3D printing to produce soft robotic fingers with discrete actuation modes and integrated ionogel soft sensors that provide proprioceptive and tactile sensing corresponding to each degree of freedom. With new readout electronics that streamline the measurement of sensor resistance, we evaluate the fingers' sensory feedback through free and blocked displacement experiments. We integrate three of our sensorized fingers together to create a soft manipulator with different grasping poses. Finally, we showcase the importance of the fingers' discrete actuation modes and integrated sensors via a closed-loop grasping study. Our methods demonstrate an enabling manufacturing platform that can be adapted to create other soft multi-DOF manipulators requiring somatosensory feedback for a variety of closed-loop and machine learning-based control algorithms.

I. INTRODUCTION

Recent developments in soft robotics have demonstrated how compliant materials can be harnessed to drive advances in robotic manipulation. From gentle [1] and universal [2] object handling to complex, bioinspired actuation motifs [3]–[6], soft robotic manipulators have demonstrated unique capabilities compared to traditional rigid manipulators [7]. Soft manipulators have widespread potential for future use in automated assembly and packaging, prosthetic devices [8], conservation [9], extreme environments, and much more [7], [10], [11]. However, creating soft robots with multi-degree-of-freedom (DOF) actuation and somatosensory capabilities remains a significant hurdle that limits their practical use in these areas [7], [10], [11].

Most soft robotic manipulators operate via open-loop control [7], [11] and have simple, single-DOF actuation, such as uniform bending or twisting [10]. Given the simplicity of fluidic actuation and molding-based fabrication techniques, fluidic elastomer actuators (FEAs) are a popular platform for producing soft manipulators. Unfortunately, these techniques require multiple assembly steps, especially when multi-DOF actuators are desired [10]. Closing the control loop on

[1]Schmidt Science Fellow

[2]MIT Computer Science and Artificial Intelligence Laboratory (CSAIL), Massachusetts Institute of Technology, Cambridge, MA, USA

[3]John A. Paulson School of Engineering and Applied Sciences, Wyss Institute for Biologically Inspired Engineering, Harvard University, Cambridge, MA, USA

*Direct email correspondence to: rltruby@mit.edu (RLT), jalewis@seas.harvard.edu (JAL), rus@csail.mit.edu (DR).
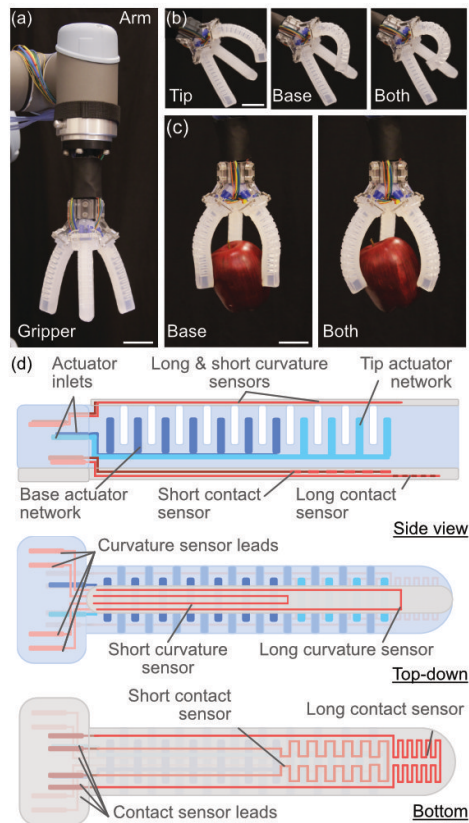
Fig. 1. Soft robotic gripper with EMB3D printed soft fingers. (a) Three fingers comprise a soft gripper fixed to a robot arm. (b) Inflating the tip (left), base (center), or tip and base (right) actuator networks enable three modes of finger bending and (c) different grasps. (d) Schematics of the finger from side (top), top-down (middle), and bottom-up (bottom) views. Scale bars are 30 mm.

manipulation requires that motion capture systems be present or sensors be integrated into the soft actuator. If sensors are incorporated, several additional design and fabrication issues arise (see *Background*).

Achieving soft somatosensitive manipulation requires an integrated design and fabrication strategy that streamlines the production of soft actuators with discrete actuation modes and integrated sensors. Here, we use embedded 3D (EMB3D) printing [12]–[15] to rapidly create soft, sensorized FEA-based fingers with multiple actuation motifs for soft manipulators (Fig. 1). As a demonstration, we print soft fingers with two discrete fluidic networks that allows for tip, base, and full-finger actuation (Fig. 1b) and multiple grasping motifs (Fig. 1c). Four soft resistive sensors - two curvature and two contact sensors - innervate each finger (Fig. 1d).

They are comprised of an organic ionogel that provides reliable sensory feedback without hysteresis in conductivity [15]. Through free and blocked displacement characterization experiments, we show that the short and long versions of the curvature and contact sensors provide proprioception and tactile sensing corresponding to the finger base and tip DOF, respectively. Finally, with a closed-loop manipulation study, we showcase how multiple grasping modes and contact sensors can improve the success of autonomous grabbing of objects. While we showcase one finger and gripper design, our platform enables the creation of a variety of soft, complex robotic manipulators for applications requiring somatosensory feedback that may be difficult or impossible to make with molding strategies alone. Altogether, our work presents the following contributions:

1) A first design for a fully 3D printed soft finger with individually addressable degrees of freedom and corresponding proprioceptive and tactile sensors,
2) A new ionogel sensor readout strategy compatible with a wide array of ionically conductive sensors that simplifies determination of resistance change, and
3) A closed-loop grasping study with soft grippers using multiple actuation modes and soft sensors.

II. BACKGROUND

Fabricating FEA-based soft robots with integrated sensors and multi-DOF actuation requires many steps. Prior work has used molding techniques to make soft quadrupeds [16], swimming fish [17], tentacle-like actuators [4], and hand-like manipulators [6], [18] with several DOF. By contrast, 3D printing offers a promising approach for rapidly designing and fabricating complex soft actuators [19]. Several light- and ink-based printing techniques have recently emerged for directly building multi-DOF soft fingers [5], legs [20], grippers [21], and integrated robotic systems [13], [22], [23].

FEAs can be innervated with rigid bend and pressure sensors [21], [24] or, alternatively, soft sensors based on liquid metals [25]–[27], conductive nanoparticle-polymer composites [28], [29], hydrogels [30]–[33], or elastomeric waveguides [8], [34]. However, conventional rigid sensors do not mechanically interface well with the soft elastomers of FEAs, nor do the rigid components required for elastomeric waveguides. Liquid metal sensors are unreliable due to the potential displacement of their passivating oxide layers over time [25]. Water evaporates from aqueous hydrogels [35]. Finally, conductive polymer composites have inconsistent conductivities due to the conductive filler's dynamic percolation network [14].

Recent work has suggested that organic ionic liquids are promising materials for robust, reliable soft robotic sensors [15], [36], [37]. However, the ionic and hygroscopic nature of the printed ionogel sensors necessitates low-voltage, AC readout strategies to bypass the effects of charge migration towards the electrodes and electrolytic side reactions in the sensors [31]. Prior embodiments with ionic sensors have relied on various signal processing strategies to measure changes in sensor impedance [15], [30], [31], [36], [37],

but these methods require specialized hardware, intrinsically limit sampling rate, and/or present computational burdens that reduces their practicality.

Embedded 3D (EMB3D) printing is a freeform fabrication method introduced by Wu and Lewis [12], which enables rapid design of soft, highly stretchable strain sensors [14], entirely soft robots [13], and soft actuators with integrated ionogel sensors [15] (Fig. 2). In EMB3D printing, one directly extrudes functional viscoelastic inks into un-crosslinked, viscoplastic matrix materials [38], which can be composed of various elastomer formulations. The inks impart embedded functionality (e.g., fluidic networks for actuation [13], [15] and conductive features for sensing [14], [15]), while the elastomeric matrix materials cure to provide the final mechanical properties of the part. The matrix materials are poured into molds that define the overall geometry of these devices.

III. SOFT MANIPULATOR DESIGN

A. Design Overview

Inspired by our bodies' sensory capabilities and manual dexterity, we designed a soft robotic gripper comprised of three FEA-based fingers possessing discrete actuation modes with soft proprioceptive and tactile sensors corresponding to each DOF in actuation. While our methods can be used to create actuators with an arbitrary number of free-form sensors and actuator networks, the devices presented in this work (Fig. 1d) have two FEA networks, a base and tip actuator network, that drive bending of the base and tip regions of the finger. The fingers' ionogel sensors, have a resistance, R_S, given by $R_S = \rho * (l/A)$, where ρ is the resistivity of the ionogel ink, l is the length of the sensor, and A is the cross-sectional area of the sensor trace. As the sensors are deformed, R_S changes. For prioprioception, short ($S_{Curve,S}$) and long curvature ($S_{Curve,L}$) sensors span the length of the base and tip actuator networks, respectively. Inflating the fingers results in elongation of the curvature sensors: $S_{Curve,S}$ is designed to increase in R_S only during inflation of the base actuator network, while $S_{Curve,L}$ undergoes the greatest change in R_S when the full finger is inflated. Short ($S_{Contact,S}$) and long contact ($S_{Contact,L}$) sensors beneath the fingertip provide tactile sensing when these features are compressed by contact pressures. $S_{Contact,L}$ is designed to indicate when contact has been made at the very tip of the
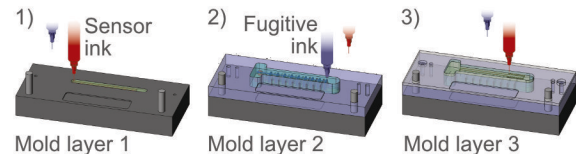

Fig. 2. EMB3D printing a sensorized soft finger. (1) The dorsal matrix is cast into the first mold layer for printing the curvature sensors with the sensor ink. (2) The second mold layer is added, and the actuator matrix is poured in for printing the actuator networks with the fugitive ink. (3) The final mold layer is added, the anterior matrix is added, and the contact sensors are printed. All sensor leads and actuator inlets are printed in the actuator matrix.

finger, and $S_{Contact,S}$ provides feedback when contact is more proximal from the tip (Fig. 1d).

Given their complex form and multi-material composition, we used EMB3D printing to fabricate our soft fingers. We print the soft sensors from an organic ionogel-based sensor ink to ensure stable, reliable perception with hysteresis-free conductivity. Finally, we designed new readout hardware for streamlined measurement of changes in sensor resistance.

B. Embedding Sensors and Actuators into Soft Fingers

The EMB3D printing technique and material sets used to manufacture our soft fingers are described in detail in our prior paper [15]. Briefly, fugitive and sensor inks are directly extruded into uncured elastomeric matrices through fine nozzles to create free-form fluidic and conductive features for actuation and sensing (Fig. 2). The fugitive ink is a viscoelastic gel of Pluronic F127 (Sigma, 25 wt% in deionized water) that exhibits a solid-to-liquid transition around 2-5°C [12]. The sensor ink is an organic ionogel comprised of 1-ethyl-3-methyl-imidazolium ethyl sulfate (Sigma) filled with 6 wt% fumed silica particles (Aerosil 380, Evonik), which impart the appropriate yield stress needed for printing [15].

Three matrix materials referred to as the dorsal, actuator, and anterior matrices are formulated from Ecoflex 10, SortaClear 40, and Ecoflex 30 silicone elastomers (Smooth-on), respectively. A cure retarder (Slo-Jo) and thixotropic additive (Thivex, both from Smooth-On) are added to impart the shear-thinning, yield-stress behavior needed for EMB3D printing [15], [38]. During printing, the matrices are poured sequentially into a multi-layer mold assembly that sets the fingers' shape (Fig. 2). The curvature sensors are first printed in the dorsal matrix. A mold layer is added, and the actuator matrix is poured in. We print the two actuator networks and sensor leads in this matrix. Finally, we add another mold layer, pour in the anterior matrix, and print the contact sensors [15].

Each finger is printed in approximately 90 min, after which it cures overnight for approximately 12 h. The fingers are then cured for 4 h at 80°C and refrigerated for 1 h to liquefy the fugitive ink. Two 22-gauge nozzles (EFD Nordson) with Luer-lock fittings are inserted into the fingers' actuator matrix, through their back end, and into the actuator network inlets. The liquified fugitive ink is aspirated with a syringe to empty the actuator networks. Ice-cold water is filled into the actuator networks to remove any Pluronic F127, and residual water is removed by heating the fingers in an oven for 2 h at 80°C.

Before use, soft fingers are wired by inserting custom leads into each sensor through the actuator matrix and into the sensor inlets. The leads are formed by soldering the ends of 28 gauge, rubber-coated wire to short nickel-plated stainless steal needles with gold electroplated tips and header pins for insertion into our readout hardware. Silicone tubing for pressurized air is fixed via the Luer lock nozzle in each of the actuator network inlets. The fingers are inflated using a MATLAB-controlled, pneumatic valve manifold (Festo)
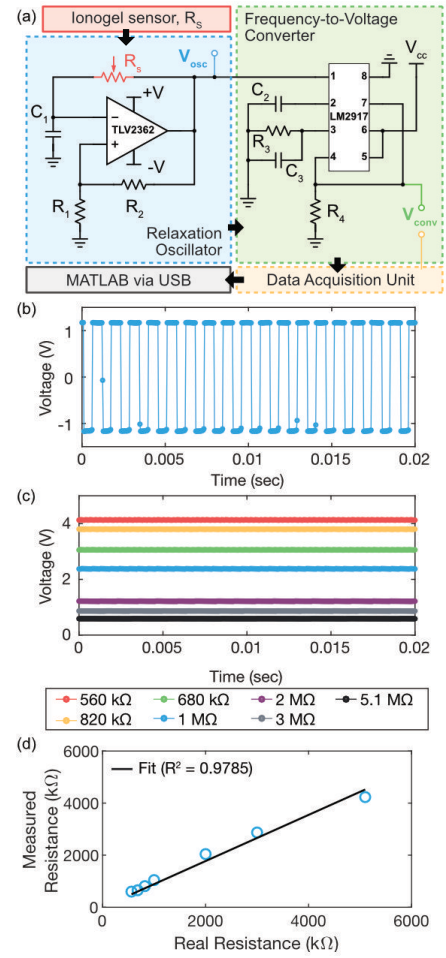

Fig. 3. Readout scheme for the embedded sensor networks. (a) Flow chart and electronics schematic for determining the resistance of an ionogel sensor, R_s. (b) The relaxation oscillator produces a signal, V_{osc}, a square wave with R_s-dependent period changes. V_{osc} for a 1 MΩ resistor is shown. (c) Various output voltage signals, V_{conv}, are shown for various resistor values from the circuit's frequency-to-voltage converter. (d) A plot of measured versus real resistance values shows that the resistance values of R_S are converted reliably by the readout electronics. The slope of the linear fit is 0.877; the intercept is 0 kΩ.

capable of independently supplying up to 200 kPa pressure from 16 different regulators.

C. Readout Electronics for Embedded Sensor Networks

Our new sensor readout strategy, shown schematically in Fig. 3a, expands on previous approaches using low-operating voltage relaxation oscillators to measure resistance change, ΔR_S, of a sensor via changes in period of the oscillator's output voltage, V_{osc} [31]. Briefly, an ionogel sensor is the resistor R_S in the relaxation oscillator's *RC* circuit (Fig. 3a). The oscillator output, V_{osc}, has the form of a square wave alternating between ±1.2V, the voltage (+V, -V) powering our op-amp (Texas Instruments TLV2362). The period, T, of V_{osc} is

$$T = 2R_sC_1 ln(\frac{1-B}{1+B}) \qquad (1)$$

where $B = R_1/(R_1 + R_2)$, C_1 is the capacitor in the *RC* circuit, and R_1 and R_2 are the resistors in the oscillator's

Schmitt trigger. $\Delta R_S = R_S - R_{S,0}$ can be determined by measuring $\Delta T = T - T_0$, where $R_{S,0}$ is the initial resistance of the sensor, and T_0 is the initial period of V_{osc}.

To avoid complex signal processing techniques that have previously been employed to solve for ΔT [31], [37], we have added a frequency-to-voltage (f-to-V) converter in series with the relaxation oscillator to simplify the determination of ΔR_S. The converter's output voltage, V_{conv}, can simply be read by a data acquisition unit (DAQ) (Fig. 3a). To interpret V_{conv}, we first note that the frequency of V_{osc} is f_{osc}, where $f_{osc} = T^{-1}$. V_{conv} is set by V_{CC} (9 V) , which powers the f-to-V converter (Texas Instruments LM2917), and the passive components R_3 and C_2:

$$V_{conv} = R_3 C_2 V_{CC} f_{osc} \qquad (2)$$

Substituting (1) into (2) shows that R_S is given by

$$R_S = \frac{R_3 C_2 V_{CC}}{2 C_1 V_{conv} ln(\frac{1-B}{1+B})} \qquad (3)$$

We designed a custom PCB with 12 copies of the electronic circuit in Fig. 3a for reading 12 soft sensors (i.e., for 3 fingers with 4 sensors per finger). Table I includes the passive component values required for our sensors. Data acquisition was performed over USB with the DAQ (National Instruments USB-6212) at a sampling frequency of 25 kHz. Calculating ΔR_S was calculated in real-time with MATLAB using (4), with $R_{S,0}$ as the initial resistance measurement of undeformed sensors. Fig. 3b shows an example of V_{osc} obtained with our readout hardware for R_S of 1 MΩ. The signal is in good agreement with (1), and Fig. 3c shows several examples of V_{conv} obtained for various resistors used as R_S. As expected from (2) and (3), R_S and V_{conv} are inversely related. Using (4) and V_{conv}, we measured the resistance of the model R_S values. A plot of measured versus real R_S values and a linear fit to the data shown in Fig. 3d confirm reliable readout of R_S values using our new readout hardware for ionogel sensors.

D. Sensorized Finger Characterization

The fingers are characterized under free and blocked displacement. For these experiments, a finger is fastened into a laser cut acrylic mount. Fingers are actuated by inflating the actuator networks in 10 kPa intervals every 30 sec. After inflation with the maximum pressure of 200 kPa, the actuator is deflated at 10 kPa intervals every 30 sec. Photographs are obtained, along with sensor readouts for 5 ms at 25 kHz, once a test pressure has held for 30 sec. For blocked displacement, short and long acrylic mounts were

Fig. 4.   Objects used in the manipulation studies. Scale bar is 50 mm.

laser cut with lengths extending from the base of the actuator to either ($S_{Contact,s}$) or ($S_{Contact,L}$), respectively. Finally, the blocked tip force was determined by actuating a finger against a mass balance with different actuation modes. The blocked force was determined as the product of the measured mass and acceleration due to gravity.

E. Gripper Assembly and Manipulation

To explore the manipulation capabilities enabled by the soft fingers, a soft gripper was constructed from three fingers oriented in a triangular orientation using a custom acrylic mount. This mount was fixed to a UR5 robot arm (Universal Robots) using a 3D printed mount (ABS Plastic, Fortus 400mc, Stratasys). For manipulation studies, objects from the collection in Fig. 4 were placed under the gripper before inflating the fingers. We also developed an algorithm (see below) for closed-loop, autonomous grasping of objects using the soft contact sensors in each finger and different grasping motifs.

IV. EXPERIMENTAL RESULTS

A. Sensorized Finger Characterization

Figs. 5a-c show a soft finger in non-inflated and inflated states where the tip, base, and full finger are inflated to 200 kPa during free (Fig. 5a) and blocked displacements with short (Fig. 5b) and long (Fig. 5c) mounts. The plots of ΔR_S determined from these experiments are provided for each sensor as a function of inflation pressure in Figs. 5d-l. Actuation occurs in less than 1 s, and ΔR_S can be calculated well under 1 ms.

During free displacement and tip-only actuation, resistance increases only for $S_{Curve,L}$, which spans nearly the entire length of the finger. No appreciable ΔR_S are observed for the other sensors (Fig. 5d). Alternatively, when only the finger base is actuated, large resistance increases in $S_{Curve,S}$ are observed as well, with ΔR_S for $S_{Curve,L}$ increasing more than during tip-only actuation (Fig. 5e). Because there are more bladders in the base actuator network than in the tip network, ΔR_S for $S_{Curve,L}$ is greater during base-only actuation. When the full finger is actuated, we see the greatest increase in ΔR_S for $S_{Curve,L}$, approximately the same ΔR_S for $S_{Curve,S}$ as during base-only inflation, and $\Delta R_S \approx 0$ kΩ for the contact sensors (Fig. 5f). Overall, during free

TABLE I

VALUES OF PASSIVE COMPONENTS FOR SENSOR READOUT
ELECTRONICS

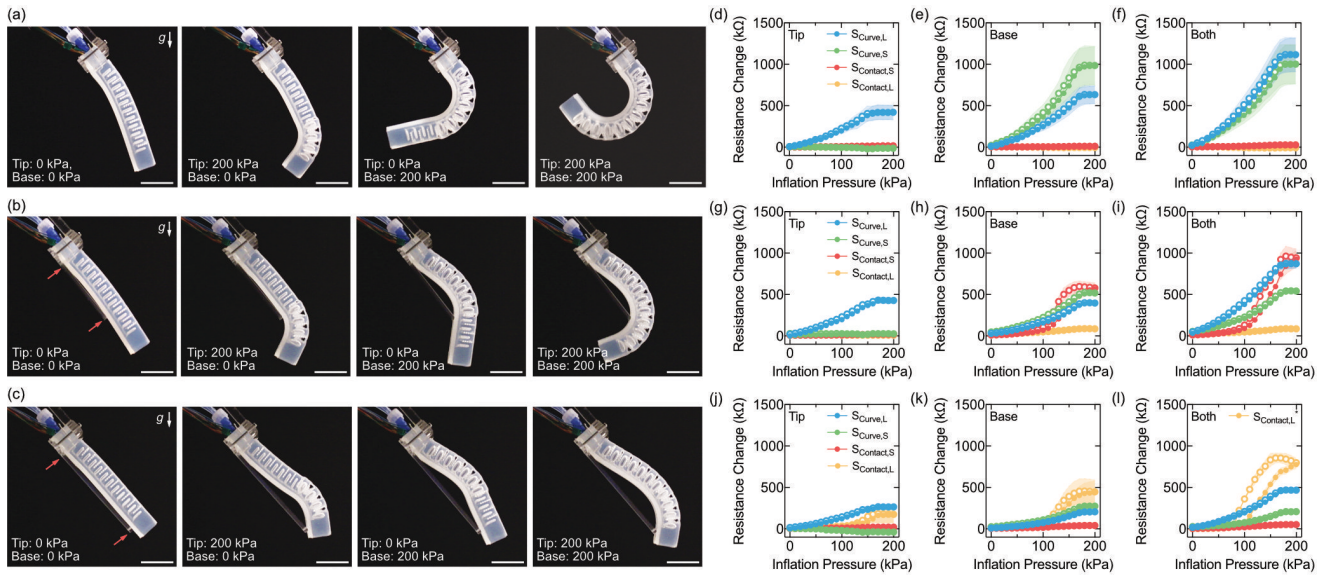| Sensor	R_1	R_2	R_3	C_1	C_2	C_3
$S_{Contact,S}$	680 Ω	10 kΩ	330 kΩ	10 nF	1 nF	1 μF
All others	680 Ω	10 kΩ	330 kΩ	4.7 nF	1 nF	1 μF

Fig. 5. Free and blocked displacement characterization of soft sensorized fingers. (a-c) Photographs of a soft finger in non-inflated (left) and various maximum inflation states for tip (center-left), base (center-right), and full (right) actuation modes during (a) free displacement and blocked displacement with the (b) short and (c) long mounts, whose edges are indicated by the red arrows. Scale bars represent 25 mm; g indicates acceleration due to gravity. (d-l) Resistance change, ΔR_S, versus inflation pressure is provided during inflation-deflation cycles (indicated by filled/open circles, respectively) for the long ($S_{Curve,L}$) and short curvature ($S_{Curve,S}$) and short ($S_{Contact,S}$) and long contact ($S_{Contact,L}$) sensors during (d-f) free displacement and blocked displacement with the (g-i) short and (j-l) long mounts. Plots correspond to ΔR_S during (d, g, j) tip, (e, h, k) base, and (f, i, l) full-finger actuation. In (l), ΔR_S for $S_{Contact,L}$ is scaled by a factor of 0.2 (to idenically scale axes across subfigures). ($n = 3$, error envelopes represent standard deviation.)

displacement of the finger in tip-only, base-only, and full-finger actuation, we observe that (i) the maximum ΔR_S for $S_{Curve,L}$ are approximately 400 kΩ, 600 kΩ, and 1100 kΩ, and (ii) the maximum ΔR_S for $S_{Curve,S}$ are approximately 0 kΩ, 1000 kΩ, and 1000 kΩ, respectively.

The soft fingers generate a force at their tip when inflated, and higher inflation pressure produces higher blocked force. We observe a maximum blocked force of approximately 550 mN generated at the tip during full-finger actuation (Fig. 6). Tip-only actuation did not provide measurable forces, and base-only actuation generated slightly lower blocked forces with inflation pressure. When the fingers are actuated against the blocking mounts, we see that the forces generated by the finger result in reduced finger bending (Figs. 5b,c).

During tip-only actuation with the short mount, we see the finger tip wraps around the mount's edge (Fig. 5b). Consequently, ΔR_S only increases appreciably for $S_{Curve,L}$
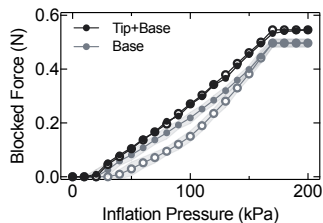

Fig. 6. Blocked force characterization. Blocked force versus inflation pressure during inflation (filled circles) and deflation cycles (open circles) of the base actuator network and full finger. ($n = 3$, error envelopes represent standard deviation.)

(Fig. 5g), with a similar magnitude to that for tip-only actuation in free displacement (Fig. 5d). During base-only actuation against the short mount, the finger presses directly into the mount, compressing $S_{Contact,S}$ and driving an increase in its resistance to approximately 600 kΩ at 200 kPa (Fig. 5h). We also see a slight increase in ΔR_S for $S_{Contact,L}$, and a clear increase in ΔR_S for $S_{Curve,S}$ (Fig. 8c). Full-finger actuation generates the most force against the short mount, driving higher increases in ΔR_S for $S_{Contact,S}$ and $S_{Curve,L}$, with a maximum ΔR_S for $S_{Contact,S}$ of about 1000 kΩ at 200 kPa (Fig. 5i). Compared to full-finger actuation in free displacement (Fig. 5f), ΔR_S slightly decreases for $S_{Curve,L}$ and nearly halves for $S_{Curve,S}$ during full actuation against the short mount because bending is constrained, especially at the finger's base region.

Finger bending is restricted even more by the long mount (Fig. 5c). Tip-only actuation drives compression of $S_{Contact,L}$, increasing its resistance and also slightly increases ΔR_S for $S_{Curve,L}$ (Fig. 5j). Base-only actuation also drives the tip against the long mount. Since base-only actuation generates a higher blocked force than tip-only actuation, we observe even higher increases in ΔR_S for $S_{Contact,L}$ (Fig. 5k). Finally, the greatest ΔR_S for $S_{Contact,L}$ is measured at approximately 3500 kΩ for full-finger actuation against the long mount at 200 kPa (Fig. 5l). $S_{Contact,S}$ does not change in resistance appreciably since the mount does not make contact with its region of the finger. Finally, the curvature sensors increase in resistance (Fig. 5l), but to a lesser extent than both free (Fig. 5f) and blocked displacement with the short mount (Fig. 5i).

To summarize, our characterization results demonstrate that the curvature sensors provide regional proprioception for each network, with $S_{Curve,S}$ only appreciably changing if the base region of the actuator is bending. The contact sensors provide regional tactile sensing, with $S_{Contact,S}$ and $S_{Contact,L}$ sensitive to compression near the end of the base and tip actuator networks, respectively. Altogether, these sensors provide feedback on the state and deformations of each DOF in our soft fingers, enabling somatosensitive manipulation.

B. Object Grasping

Our 3-finger gripper provides different grasp motifs during base-only and full-finger actuation (Fig. 7). Examples of our gripper holding objects are shown in Fig. 8. These objects were hand-fed to the gripper, which inflated around them without sensory feedback. When grasping with base-only actuation, the gripper's fingers hold the object with a larger portion of the tip pressing against the object, increasing opportunities for both contact sensors to increase in resistance. When the full finger is inflated, we tend to see the gripper hold objects by just the fingertips, only increasing ΔR_S for $S_{Contact,L}$ (Figs. 1c, 8a-b) [39]. Some objects, like those in Fig. 8c, can be held by our gripper when positioned in specific orientations before finger actuation. These objects had a thin or high-aspect ratio profile, were too heavy, and/or were either much larger than the gripper or too small to hold. Grasping results with base-only and full actuation of the fingers at 140 kPa are provided in Table II for all objects in Fig. 4. Items that were successfully gripped in both cases were lightweight and easy for the gripper to pick up just by the fingertips. While we chose a moderate inflation pressure for all manipulation studies, the gripper could hold all of the items with full-finger inflation at pressures above 180 kPa.

C. Closed-Loop Object Picking

When our gripper grabs with full-finger actuation, the fingers rarely hold objects right against both contact sensors. By contrast, good contact between the contact sensors and an object can occur with base-only actuation (Figs. 1c, 8a-b), increasing both contact sensors' resistances. However, depending on how contact is made with an object, full-finger actuation can generate sufficiently high contact forces to increase resistance of both contact sensors, even though the object is not pressing directly against both.
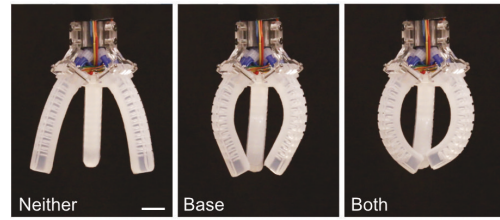

Fig. 7. Examples of manipulator poses. Photographs of the soft gripper during no (left), base-only (center), and full-finger actuation at inflation pressures of 140 kPa. Scale bar is 15 mm.
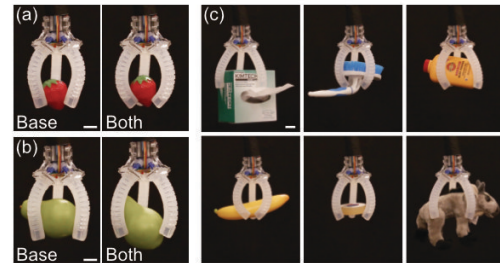

Fig. 8. Examples of object grasping. (a-b) Examples of grasping poses are shown for holding a toy strawberry (a) and pear (b) during base-only (left) and full-finger actuation (right). (c) Examples of objects that can be grasped by the soft gripper with appropriate pre-grasp orientation. Inflation pressure is 140 kPa in each photograph. Scale bars are 15 mm.

To showcase the value of having discrete control over base and tip actuation of our fingers during autonomous, closed-loop grasping, we developed Algorithm 1 to autonomously grab an object placed underneath our gripper. The general idea is to use base-only or full finger actuation to probe finger contact and guide finger placement around the object such that the fingers were able to robustly grab and lift it.

With Algorithm 1, we attempted to grab each object in Fig. 4. Briefly, the gripper moves down over an object on a table, inflating the fingers via base-only or full actuation to probe whether a finger has made contact with the object. Contact with a finger is noted when both $S_{Contact,S}$ and $S_{Contact,L}$ have exceeded a critical resistance change, $\Delta R_{S,crit}$, which is 8 kΩ and 20 kΩ, respectively. We use this rule to guide the gripper to a proper length down the object for successful lifting off the table. If all three fingers have made contact during the grasp attempt, then the fingers are inflated fully, and the gripper moves upward to lift the object off the table.

TABLE II
SUMMARY OF GRASPING RESULTS AT 140 KPA

Grasping Motif	Plush Toy	Lab Wipes	Baby Powder	Bubble Wrap	Soda Can	Chips
Base-only Actuation	Fail	Success	Fail	Success	Success	Success
Full-finger Actuation	Success	Success	Success	Success	Success	Success
Grasping Motif	Pear	Apple	Banana	Strawberry	Dish Brush	Baking Pin
Base-only Actuation	Success	Success	Fail	Success	Fail	Fail
Full-finger Actuation	Success	Success	Success	Success	Success	Fail
Grasping Motif	Cleaning Wipes	Cube	Big Tape	Small Tape	Coffee Mug	Zip Ties
Base-only Actuation	Fail	Success	Fail	Success	Success	Fail
Full-finger Actuation	Fail	Success	Fail	Success	Success	Fail

Algorithm 1 Closed-Loop Object Picking

1: Move to gripper's starting height
2: **while** < 3 fingers have made contact & gripper can move down 20 mm **do**
3:    **while** Inflation pressure <140 kPa **do**
4:       Increase actuation pressure by 10 kPa, using
5:       base-only or full-finger actuation
6:       **if** Finger N's contact sensors are $>\Delta R_{S,crit}$ **then**
7:          Finger N made contact
8:    **if** < 3 fingers have made contact **then**
9:       Deflate all fingers & move gripper down
10:      20 mm if able to
11: **if** < 3 fingers made contact during grab attempt **then**
12:    **if** 2 fingers made contact **then**
13:       Inflate fingers to 140 kPa (full actuation), lift to
14:       pick up off table
15:    **else** Lift non-inflated gripper to starting height
16: **else** Inflate fingers at 140 kPa (full actuation), lift to
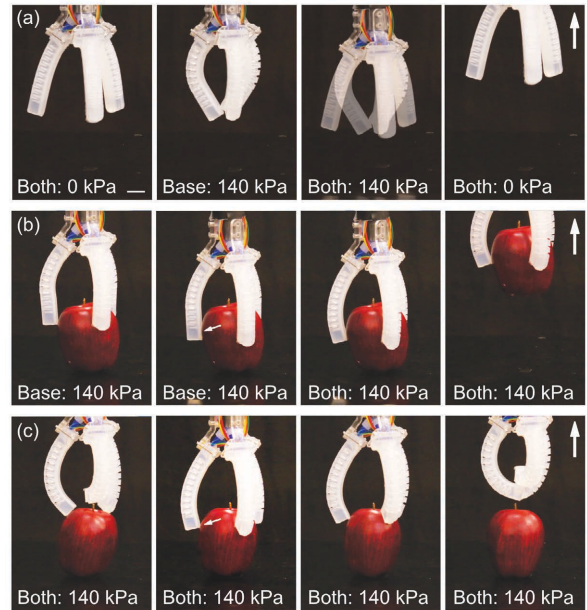17:   pick up off table

Fig. 9. Examples of autonomous grabbing. Photographs of the gripper using Algorithm 1 to autonomously pick up a toy apple. (a) With no apple present, the gripper periodically inflates and probes downward for an object. The fourth image shows a non-actuated gripper moving back to its starting height. (b,c) Photographs illustrate the results when (b) base-only or (c) full-finger actuation are used to probe contact. Here, the first images show a representative probing actuation. The second image shows the grasping attempt at which contact in all fingers has been made. The small white arrows show how the fingers make contact with the surface of the apple at this step. The third image shows all fingers fully inflated, and the last shows the result as the robot lifts upward. In (a)-(c), the large arrows in the fourth image indicate that the gripper is raising upwards. Scale bar is 15 mm.

If the gripper has moved down as far as it safely can and two fingers made contact at the end of the grasp attempt, we still fully actuate all fingers, and the gripper will try to lift the object off the table. Fig. 9 shows photographs from trials when no item is present (Fig. 9a) or when a plastic apple is under the gripper, where base-only (Fig. 9b) or full-finger actuation (Fig. 9c) is used to probe for finger contact. By positioning the gripper for a grab using base-only actuation first, we observed that the robot arm was able to position the gripper further down the apple to ensure a more robust grab and, thus, successful lift. Results from closed-loop grasping trials are provided in Table III for other objects and show that selective control over finger actuation can enable more successful grabs guided by tactile feedback. For this study, we excluded items that could not be held during open-loop grasping with base-only actuation at 140 kPa (see Table II). These items were too thin, heavy, or short for our current set-up and gripper design. Again, we chose a moderate inflation pressure for these studies, and higher pressures enabled us to lift some of the other objects.

V. CONCLUSIONS AND FUTURE WORK

Our work represents a first study in fabricating, characterizing, and utilizing multi-DOF, soft robotic fingers with embedded soft sensors for closed-loop, somatosensitive manipulation. The fingers have two degrees of freedom enabled by base and tip actuator networks and four ionogel sensors that provide discrete proprioceptive and tactile senses that correspond to each DOF. We made our soft robotic fingers using a versatile additive manufacturing technique known as EMB3D printing that allows one to arbitrarily pattern the actuation, sensory, and elastomeric features required for our finger design in a modular way. Finally, we developed an algorithm for our soft gripper to autonomously grasp objects using its discrete actuation modes and embedded sensors.

We are now actively pursuing new multi-DOF, sensorized soft actuator designs using these methods to create more complex types of dexterous, soft robotic manipulators. Soft manipulator designs that we are exploring have different finger numbers, orientations, designs, and sensing motifs than the gripper presented here. Working with established algorithms in grasp planning with soft grippers [40] and object recognition [29], we aim to develop soft robots with advanced manipulation capabilities that will be useful in myriad applications.

TABLE III
SUMMARY OF CLOSED-LOOP GRASPING RESULTS AT 140 KPA

Experiment	Plush Toy	Lab Wipes	Soda Can	Chips	Cube	Coffee Mug	Pear	Apple
Grasp Guided by Full-Finger Actuation	Success	Fail	Success	Success	Fail	Fail	Fail	Fail
Grasp Guided by Base-Only Actuation	Success	Success	Success	Success	Success	Success	Success	Success

328

REFERENCES

[1] F. Ilievski, A. D. Mazzeo, R. F. Shepherd, X. Chen, and G. M. Whitesides, "Soft Robotics for Chemists," *Angewandte Chemie - International Edition*, vol. 123, pp. 1930–1935, 2011.

[2] E. Brown, N. Rodenberg, J. Amend, A. Mozeika, E. Steltz, M. R. Zakin, H. Lipson, and H. M. Jaeger, "Universal robotic gripper based on the jamming of granular material," *PNAS*, vol. 107, no. 44, pp. 18 809–18 814, 2010.

[3] C. Laschi, M. Cianchetti, B. Mazzolai, L. Margheri, M. Follador, and P. Dario, "Soft robot arm inspired by the octopus," *Advanced Robotics*, vol. 26, no. 7, pp. 709–727, 2012.

[4] R. V. Martinez, J. L. Branch, C. R. Fish, L. Jin, R. F. Shepherd, R. M. Nunes, Z. Suo, and G. M. Whitesides, "Robotic tentacles with three-dimensional mobility based on flexible elastomers," *Advanced Materials*, vol. 25, pp. 205–212, 2013.

[5] B. N. Peele, T. J. Wallin, H. Zhao, and R. F. Shepherd, "3D printing antagonistic systems of artificial muscle using projection stereolithography," *Bioinspiration & Biomimetics*, vol. 10, p. 055003, 2015.

[6] J. Zhou, J. Yi, X. Chen, Z. Liu, and Z. Wang, "BCL-13: A 13-DOF Soft Robotic Hand for Dexterous Grasping and In-hand Manipulation," *IEEE Robotics and Automation Letters*, vol. 3, no. 4, pp. 3379–3386, 2018.

[7] J. Shintake, V. Cacucciolo, D. Floreano, and H. Shea, "Soft Robotic Grippers," *Advanced Materials*, vol. 30, no. 29, p. 1707035, 2018.

[8] H. Zhao, K. O'Brien, S. Li, and R. F. Shepherd, "Optoelectronically innervated soft prosthetic hand via stretchable optical waveguides," *Science Robotics*, vol. 1, p. eaai7529, 2016.

[9] K. C. Galloway, K. P. Becker, B. Phillips, J. Kirby, S. Licht, D. Tchernov, R. J. Wood, and D. F. Gruber, "Soft Robotic Grippers for Biological Sampling on Deep Reefs," *Soft Robotics*, vol. 3, no. 1, pp. 23–33, 2016.

[10] B. Gorissen, D. Reynaerts, S. Konishi, K. Yoshida, J. W. Kim, and M. De Volder, "Elastic Inflatable Actuators for Soft Robotic Applications," *Advanced Materials*, vol. 29, no. 43, p. 1604977, 2017.

[11] H. Wang, M. Totaro, and L. Beccai, "Toward Perceptive Soft Robots: Progress and Challenges," *Advanced Science*, vol. 5, p. 1800541, 2018.

[12] W. Wu, A. Deconinck, and J. A. Lewis, "Omnidirectional printing of 3D microvascular networks," *Advanced Materials*, vol. 23, no. 24, pp. H178–H183, 2011.

[13] M. Wehner, R. L. Truby, D. J. Fitzgerald, B. Mosadegh, G. M. Whitesides, J. A. Lewis, and R. J. Wood, "An integrated design and fabrication strategy for entirely soft, autonomous robots," *Nature*, vol. 536, no. 7617, pp. 451–455, 2016.

[14] J. T. Muth, D. M. Vogt, R. L. Truby, Y. Meng, D. B. Kolesky, R. J. Wood, and J. A. Lewis, "Embedded 3d printing of strain sensors within highly stretchable elastomers," *Advanced Materials*, vol. 26, no. 36, pp. 6307–6312.

[15] R. L. Truby, M. Wehner, A. K. Grosskopf, D. M. Vogt, S. G. Uzel, R. J. Wood, and J. A. Lewis, "Soft Somatosensitive Actuators via Embedded 3D Printing," *Advanced Materials*, vol. 30, no. 15, p. 1706383, 2018.

[16] R. F. Shepherd, F. Ilievski, W. Choi, S. A. Morin, A. A. Stokes, A. D. Mazzeo, X. Chen, M. Wang, and G. M. Whitesides, "Multigait soft robot," *PNAS*, vol. 108, no. 51, pp. 20 400–20 403, 2011.

[17] R. K. Katzschmann, J. DelPreto, R. MacCurdy, and D. Rus, "Exploration of underwater life with an acoustically controlled soft robotic fish," *Science Robotics*, vol. 3, no. 16, 2018.

[18] J. Zhou, S. Chen, and Z. Wang, "A Soft-Robotic Gripper With Enhanced Object Adaptation and Grasping Reliability," *IEEE Robotics and Automation Letters*, vol. 2, no. 4, pp. 2287–2293, 2017.

[19] T. J. Wallin, J. Pikul, and R. F. Shepherd, "3D printing of soft robotic systems," *Nature Reviews Materials*, vol. 3, no. 6, pp. 84–100, 2018.

[20] D. Drotman, S. Jadhav, M. Karimi, P. DeZonia, and M. T. Tolley, "3D printed soft actuators for a legged robot capable of navigating unstructured terrain," in *2017 IEEE International Conference on Robotics and Automation (ICRA)*, 2017, pp. 5532–5538.

[21] Z. Wang and S. Hirai, "A 3D printed soft gripper integrated with curvature sensor for studying soft grasping," in *2016 IEEE/SICE International Symposium on System Integration*, 2016, pp. 629–633.

[22] N. W. Bartlett, M. T. Tolley, J. T. B. Overvelde, J. C. Weaver, B. Mosadegh, K. Bertoldi, G. M. Whitesides, and R. J. Wood, "A 3D-printed, functionally graded soft robot powered by combustion," *Science*, vol. 349, no. 6244, pp. 161–165, 2015.

[23] C. MacCurdy, R. Katzschmann, Y. Kim, D. Rus, and R. MacCurdy, "Printable Hydraulics: A Method for Fabricating Robots by 3D Co-Printing Solids and Liquids," in *IEEE International Conference on Robotics and Automation (ICRA)*, 2016, pp. 3878–3885.

[24] B. S. Homberg, R. K. Katzchmann, M. R. Dogar, and D. Rus, "Haptic Identification of Objects using a Modular Soft Robotic Gripper," in *2015 IEEE/RSJ International Conference on Intelligent Robots and Systems (IROS)*, 2015, pp. 1698–1705.

[25] R. Adam Bilodeau, E. L. White, and R. K. Kramer, "Monolithic fabrication of sensors and actuators in a soft robotic gripper," in *IEEE International Conference on Intelligent Robots and Systems (IROS)*, 2015, pp. 2324–2329.

[26] J. Morrow, H. S. Shin, C. Phillips-Grafflin, S. H. Jang, J. Torrey, R. Larkins, S. Dang, Y. L. Park, and D. Berenson, "Improving Soft Pneumatic Actuator Fingers through Integration of Soft Sensors, Position and Force Control, and Rigid Fingernails," in *IEEE International Conference on Robotics and Automation (ICRA)*, 2016, pp. 5024–5031.

[27] V. Wall, G. Zoller, and O. Brock, "A method for sensorizing soft actuators and its application to the RBO hand 2," in *2017 IEEE International Conference on Robotics and Automation (ICRA)*, 2017, pp. 4965–4970.

[28] K. Kure, T. Kanda, K. Suzumori, and S. Wakimoto, "Intelligent FMA using flexible displacement sensor with paste injection," in *IEEE International Conference on Robotics and Automation (ICRA)*, 2006, pp. 1012–1017.

[29] B. Shih, D. Drotman, C. Christianson, Z. Huo, R. White, H. I. Christensen, and M. T. Tolley, "Custom soft robotic gripper sensor skins for haptic object visualization," in *IEEE International Conference on Intelligent Robots and Systems*, vol. 2017-Septe, 2017, pp. 494–501.

[30] P. Manandhar, P. D. Calvert, and J. R. Buck, "Elastomeric ionic hydrogel sensor for large strains," *IEEE Sensors Journal*, vol. 12, no. 6, pp. 2052–2061, 2012.

[31] J. B. Chossat, Y. L. Park, R. J. Wood, and V. Duchaine, "A soft strain sensor based on ionic and metal liquids," *IEEE Sensors Journal*, vol. 13, no. 9, pp. 3405–3414, 2013.

[32] C. Larson, B. Peele, S. Li, S. Robinson, M. Totaro, L. Beccai, B. Mazzolai, and R. Shepherd, "Highly stretchable electroluminescent skin for optical signaling and tactile sensing," *Science*, vol. 351, no. 6277, pp. 1071–1074, 2016.

[33] D. Y. Choi, M. H. Kim, Y. S. Oh, S. H. Jung, J. H. Jung, H. J. Sung, H. W. Lee, and H. M. Lee, "Highly stretchable, hysteresis-free ionic liquid-based strain sensor for precise human motion monitoring," *ACS Applied Materials and Interfaces*, vol. 9, no. 2, pp. 1770–1780, 2017.

[34] S. Sareh, Y. Noh, M. Li, T. Ranzani, H. Liu, and K. Althoefer, "Macrobend optical sensing for pose measurement in soft robot arms," *Smart Materials and Structures*, vol. 24, p. 125024, 2015.

[35] H. Yuk, T. Zhang, G. A. Parada, X. Liu, and X. Zhao, "Skin-inspired hydrogel-elastomer hybrids with robust interfaces and functional microstructures," *Nature Communications*, vol. 7, p. 12028, 2016.

[36] J. B. Chossat, Y. Tao, V. Duchaine, and Y. L. Park, "Wearable soft artificial skin for hand motion detection with embedded microfluidic strain sensing," in *2015 IEEE International Conference on Robotics and Automation (ICRA)*, 2015, pp. 2568–2573.

[37] J.-B. Chossat, H.-S. Shin, Y.-L. Park, and V. Duchaine, "Soft Tactile Skin Using an Embedded Ionic Liquid and Tomographic Imaging," *Journal of Mechanisms and Robotics*, vol. 7, p. 021008, 2015.

[38] A. K. Grosskopf, R. L. Truby, H. Kim, A. Perazzo, J. A. Lewis, and H. A. Stone, "Viscoplastic Matrix Materials for Embedded 3D Printing," *ACS Applied Materials and Interfaces*, vol. 10, no. 27, pp. 23 353–23 361, 2018.

[39] P. Glick, S. Suresh, D. Ruffatto III, M. Cutkosky, M. T. Tolley, and A. Parness, "A soft robotic gripper with gecko-inspired adhesive," *IEEE Robotics and Automation Letters*, vol. 3, no. 2, pp. 903–910, 2018.

[40] C. Choi, W. Schwarting, J. DelPreto, and D. Rus, "Learning Object Grasping for Soft Robot Hands," *IEEE Robotics and Automation Letters*, vol. 3, no. 3, pp. 2370–2377, 2018.